

# Deep learning for undersampled MRI reconstruction

Chang Min Hyun\*, Hwa Pyung Kim\*, Sung Min Lee\*, Sungchul Lee<sup>†</sup> and Jin Keun Seo\*

\* Department of Computational Science and Engineering, Yonsei University, Seoul, 03722, South Korea

<sup>†</sup> Department of Mathematics, Yonsei University, Seoul, 03722, South Korea

**Abstract**—This paper presents a deep learning method for faster magnetic resonance imaging (MRI) by reducing  $k$ -space data with sub-Nyquist sampling strategies and provides a rationale for why the proposed approach works well. Uniform subsampling is used in the time-consuming phase-encoding direction to capture high-resolution image information, while permitting the image-folding problem dictated by the Poisson summation formula. To deal with the localization uncertainty due to image folding, very few low-frequency  $k$ -space data are added. Training the deep learning net involves input and output images that are pairs of Fourier transforms of the subsampled and fully sampled  $k$ -space data. Numerous experiments show the remarkable performance of the proposed method; only 29% of  $k$ -space data can generate images of high quality as effectively as standard MRI reconstruction with fully sampled data.

**Index Terms**—Magnetic resonance imaging, Fast MRI, Deep learning, Undersampling.

## I. INTRODUCTION

Magnetic resonance imaging (MRI) produces cross-sectional images with high spatial resolution by using strong nuclear magnetic resonances, gradient fields, and hydrogen atoms inside the human body [8], [15]. MRI does not use damaging ionizing radiation like X-rays, but the scan takes a long time and involves confining the subject in an uncomfortable narrow tube. While shortening the MRI scan time does not reduce radioactive iodine dosage, it might help increase patients' treatment satisfaction and reduce the medical cost. The MRI scan time is roughly proportional to the number of time-consuming phase-encoding steps in  $k$ -space. Many efforts have sought to expedite MRI scans by skipping phase-encoding lines in  $k$ -space while eliminating aliasing, a serious consequence of the Nyquist criteria violation [11] caused by skipping. To eliminate or ease aliasing, we use prior information on MR images of the missing  $k$ -space data. Parallel MRI and compressed MRI are some of the techniques used to deal with these aliasing artifacts. Parallel MRI installs multiple receiver coils and uses space-dependent properties of receiver coils to ease aliasing [7], [12], [16]. This paper focuses solely on undersampled MRI; for simplicity, parallel MRI will not be discussed.

Undersampled MRI aims to produce medically acceptable high quality images as good as fully sampled MRI using undersampled MRI data. Undersampled MRI consists of two parts, the subsampling and reconstruction, as shown in Fig.1. The subsampling systematically reduces the original MRI  $k$ -space data  $\mathbf{x}_{\text{full}}$  to the undersampled data  $\mathbf{x}$ . Reconstruction involves learning the optimal reconstruction function  $f : \mathbf{x} \mapsto \mathbf{y}$ ,

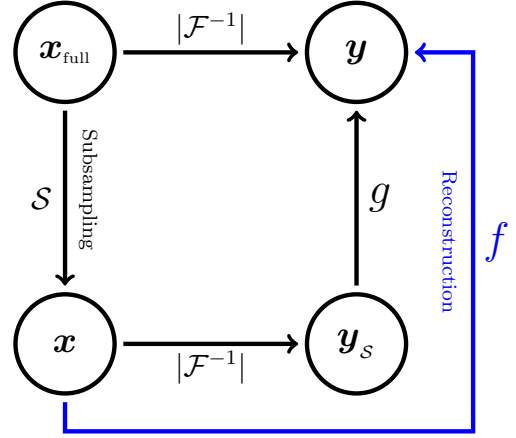


Fig. 1. General strategy for undersampled MRI reconstruction problem. The inverse Fourier transform ( $|\mathcal{F}^{-1}|$ ) of a fully sampled  $k$ -space data  $\mathbf{x}_{\text{full}}$  produces a reconstructed MRI image  $\mathbf{y}$ . The goal is to find a subsampling function  $\mathcal{S}$  and learn an undersampled MRI reconstruction  $f$  from training data set. Here,  $\mathbf{y}_s = |\mathcal{F}^{-1}|(\mathbf{x})$  is an aliased image caused by the violation of Nyquist criteria. We use the U-net to find the function  $g$  which provides the mapping from the aliased image  $\mathbf{y}_s$  to an anti-aliased image  $\mathbf{y}$ .

where  $\mathbf{y}$  is the MR image of the original MRI  $k$ -space data  $\mathbf{x}_{\text{full}}$ . One should note that this reconstruction function  $f$  cannot fully recover the original MR image  $\mathbf{y}$  from the undersampled data  $\mathbf{x}$ .  $f(\mathbf{x})$  only approximates  $\mathbf{y}$ . The reconstructed image  $f(\mathbf{x})$  should approximate the full MR image  $\mathbf{y}$  with medically acceptable tolerance. To minimize the reconstruction error, we must design the subsampling such that it preserves the information in  $\mathbf{x}_{\text{full}}$  as much as possible. On the other hand, to shorten MRI scan time, we must design the subsampling with high skipping rate. In this paper we balance these two and propose a subsampling that uses only 29% of the original data. We use the deep learning technique, more specifically the U-net [13] with some domain knowledge to construct the optimal reconstruction function  $f$ .

Compressive sensing (CS) MRI can be viewed as a method beyond the Nyquist requirement, in which the image sparsity is enforced to compensate for highly undersampled data [1], [10]. CS-MRI can be described roughly as a model-fitting method to reconstruct the MR image  $\mathbf{y}$  by adding a regularization term that enforces the sparsity-inducing prior on  $\mathbf{y}$ . It aims to reconstruct an image given by

$$\mathbf{y} = \underset{\mathbf{y}}{\operatorname{argmin}} \|\mathbf{x} - \mathcal{S} \circ \mathcal{F}(\mathbf{y})\|_{\ell_2}^2 + \lambda \|\mathcal{T}(\mathbf{y})\|_{\ell_1}, \quad (1)$$

where  $\mathcal{F}$  denotes the Fourier transform,  $\mathcal{S}$  is a subsampling,  $\mathcal{T}(\mathbf{y})$  represents a transformation capturing the sparsity pattern

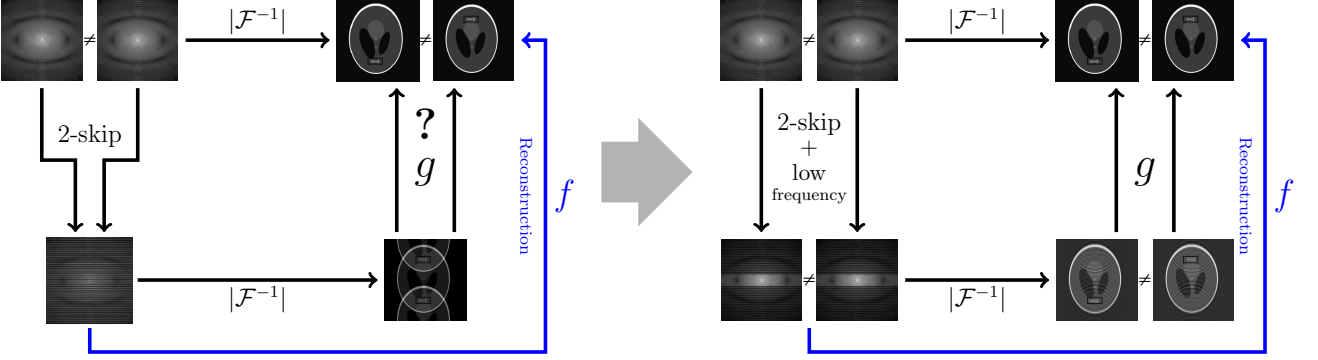


Fig. 2. Feasibility of deep learning methods. Learning  $f$  requires separability:  $\mathbf{y}_1 \neq \mathbf{y}_2$  implies  $\mathcal{S} \circ \mathcal{F}(\mathbf{y}_1) \neq \mathcal{S} \circ \mathcal{F}(\mathbf{y}_2)$ . The figure on the left shows how uniform subsampling does not satisfy the separability condition. We consider two different MR images with small anomalies at position  $(n, m)$  and  $(n, m + N/2)$ , respectively. Corresponding  $k$ -space data are different, but corresponding 2-skip  $k$ -space data are completely identical. There is no way to identify whether the anomaly is at the top or bottom from these two identical 2-skip  $k$ -space data. In contrast, the figure on the right shows how separability can be achieved by adding low frequency data.

of  $\mathbf{y}$ ,  $\circ$  is the symbol of composition, and  $\lambda$  is the regularization parameter controlling the trade-off between the residual norm and regularity. Here, the term  $\|\mathbf{x} - \mathcal{S} \circ \mathcal{F}(\mathbf{y})\|_{\ell_2}$  forces the residual  $\mathbf{x} - \mathcal{S} \circ \mathcal{F}(\mathbf{y})$  to be small, whereas  $\|\mathcal{T}(\mathbf{y})\|_{\ell_1}$  enforces the sparsity of  $\mathcal{T}(\mathbf{y})$ .

In CS-MRI, a priori knowledge of MR images is converted to a sparsity of  $\mathcal{T}(\mathbf{y})$  with a suitable choice of  $\mathcal{T}$ . The most widely used CS method is total variation denoising (i.e.,  $\|\nabla \mathbf{y}\|_{\ell_1}$ ), which enforces piecewise constant images by uniformly penalizing image gradients. Although CS-MRI with random sampling has gained great attention over the past decade, it has some limitations in preserving fine-scale details and noise-like textures that hold diagnostically important information in MR images.

In contrast to the regularized least square approaches (1), our deep learning approach is a completely reversed paradigm. It aims to learn a function  $f : \mathbf{x} \mapsto \mathbf{y}$  using many training data  $\{(\mathbf{x}^{(i)}, \mathbf{y}^{(i)}) : i = 1, \dots, N\}$ . Roughly speaking,  $f$  is achieved by

$$f = \underset{f \in \mathbb{U}_{net}}{\operatorname{argmin}} \frac{1}{N} \sum_{i=1}^N \|f(\mathbf{x}^{(i)}) - \mathbf{y}^{(i)}\|^2, \quad (2)$$

where  $\mathbb{U}_{net}$  is a deep convolutional neural network with some domain knowledge. This reconstruction function  $f$  can be viewed as the inverse mapping of the forward model  $\mathcal{S} \circ \mathcal{F}$  subject to the constraint of MR images, which are assumed to exist in a low dimensional manifold. In the conventional regularized least square framework (1), it is very difficult to incorporate the very complicated MR image manifold in the regularization term. However, in the deep learning framework, the manifold constraint learned from the training set acts as a highly nonlinear compressed sensing to get an useful reconstruction  $f(\mathbf{x})$  by leveraging complex prior knowledge on  $\mathbf{y}$ .

This paper shows that a suitably chosen subsampling with deep learning produces high-quality MR images as effectively as regular MRI reconstruction from fully sampled  $k$ -space data. To be precise, we skip four phase-encoding lines so that the Fourier transform contains all detailed features in a 4-

folded image, according to the Poisson summation formula. We include 4% low-frequency sampling to learn the overall structure of MR images. Numerous experiments show the remarkable performance of the proposed method.

## II. METHOD

Let  $\mathbf{y} \in \mathbb{C}^{N \times N}$  be the MR image to be reconstructed, where  $N^2$  is the number of pixels and  $\mathbb{C}$  is the set of complex numbers. In 2D Fourier imaging with conventional Cartesian  $k$ -space sampling, the MR image  $\mathbf{y}$  can be reconstructed from the corresponding  $k$ -space data  $\mathbf{x}_{\text{full}} \in \mathbb{C}^{N \times N}$ : For  $n, m = 1 - N/2, \dots, 0, \dots, N/2$ ,

$$\mathbf{y}(n, m) = \sum_{a=1-N/2}^{N/2} \sum_{b=1-N/2}^{N/2} \mathbf{x}_{\text{full}}(a, b) e^{2i\pi(an+bm)/N}, \quad (3)$$

where  $\mathbf{x}_{\text{full}}(a, b)$  is the MR-signal received at  $k$ -space position  $(2\pi a/N, 2\pi b/N)$ . The frequency-encoding is along  $a$ -axis in  $k$ -space and the phase-encoding is along  $b$ -axis as per our convention.

In undersampled MRI, we violate the Nyquist criteria and skip phase-encoding lines during MRI acquisition to speed up the time-consuming phase encoding. Further, we use prior information on MR images and reconstruct the image from undersampled data. However, sub-Nyquist  $k$ -space data results in aliasing artifacts in the image space. For example, suppose we skip two phase-encoding lines and get an acceleration factor of 2. Then, the  $k$ -space data with zero padding is given by

$$\begin{pmatrix} \dots & \mathbf{x}_{\text{full}}\left(\frac{N}{2} - 1, \frac{N}{2}\right) & \mathbf{x}_{\text{full}}\left(\frac{N}{2}, \frac{N}{2}\right) \\ \dots & 0 & 0 \\ \dots & \mathbf{x}_{\text{full}}\left(\frac{N}{2} - 1, \frac{N}{2} - 2\right) & \mathbf{x}_{\text{full}}\left(\frac{N}{2}, \frac{N}{2} - 2\right) \\ \dots & 0 & 0 \\ \vdots & \vdots & \vdots \end{pmatrix}. \quad (4)$$

According to the Poisson summation formula, the discrete Fourier transform of the above skipped data produces the following two-folded image:

$$\mathbf{y}_{2\text{-fold}}(n, m) = \mathbf{y}(n, m) + \mathbf{y}(n, m + N/2). \quad (5)$$

If the deep learning approach finds an unfolding map  $\mathbf{y}_{2\text{-fold}} \mapsto \mathbf{y}$ , we can accelerate the data acquisition speed. However, it is impossible to get this unfolding map even with sophisticated manifold learning for MR images. In the left panel of Fig. 2, we consider two different MR images with small anomalies at position  $(n, m)$  and  $(n, m + N/2)$ , respectively. As a result, the corresponding  $k$ -space data are different. However, the corresponding 2-skip  $k$ -space data are completely identical. There is no way to identify whether the anomaly is at the top or bottom from these two identical 2-skip  $k$ -space data. Deep learning cannot make impossible possible. Now, we are ready to explain our undersampling strategy for deep learning.

#### A. Subsampling Strategy

Let  $\{(\mathbf{x}^{(j)}, \mathbf{y}^{(j)})\}_{j=1}^M$  be a training set of undersampled and ground-truth MR images. The vectors  $\mathbf{x}^{(j)}$  and  $\mathbf{y}^{(j)}$  exist in the space  $\mathbb{C}^{N \times N}$ .

Fig. 1 shows a schematic diagram of our undersampled reconstruction method, where the corresponding inverse problem is to solve the underdetermined linear system,

$$\mathcal{S} \circ \mathcal{F}(\mathbf{y}) = \mathbf{x}. \quad (6)$$

Given undersampled data  $\mathbf{x}$ , there are infinitely many solutions in the space  $\mathbb{C}^{N \times N}$  satisfying (6). In other word, it is impossible to invert the ill-conditioned system  $\mathcal{S} \circ \mathcal{F} : \mathbb{C}^{N \times N} \rightarrow \mathcal{R}_{\mathcal{S} \circ \mathcal{F}}$ , where  $\mathcal{R}_{\mathcal{S} \circ \mathcal{F}}$  is the range space of operator  $\mathcal{S} \circ \mathcal{F}$  and its dimension is much lower than  $N^2$ . We must use the fact that the MR images of humans exist in a much lower dimensional manifold  $\mathcal{M}$  embedded in the space  $\mathbb{C}^{N \times N}$ . With this constraint  $\mathcal{M}$  which is unknown, there is a possibility that there exists a practically meaningful inverse  $f$  in the sense that

$$f(\mathcal{S} \circ \mathcal{F}(\mathbf{y})) = \mathbf{y} \quad \text{for } \mathbf{y} \in \mathcal{M}. \quad (7)$$

The major issue is what types of subsampling  $\mathcal{S}$  allow to learn  $f$  from the corresponding training data. To learn  $f$  that meets the condition (7), the subsampling  $\mathcal{S}$  must satisfy the following separability condition: for  $\mathbf{y}_1, \mathbf{y}_2 \in \mathcal{M}$ ,

$$\mathbf{y}_1 \neq \mathbf{y}_2 \text{ implies } \mathcal{S} \circ \mathcal{F}(\mathbf{y}_1) \neq \mathcal{S} \circ \mathcal{F}(\mathbf{y}_2). \quad (8)$$

The image on the left in Fig. 2 shows the case what  $\mathcal{S}$  is the 2-skipped subsampling. With this choice of  $\mathcal{S}$ , two different images  $\mathbf{y}_1 \neq \mathbf{y}_2$  produce the same  $\mathcal{S} \circ \mathcal{F}(\mathbf{y}_1) = \mathcal{S} \circ \mathcal{F}(\mathbf{y}_2)$ . This means that the 2-skipped subsampling is inappropriate to learn  $f$  satisfying (7). Here,  $\mathbf{y}_1$  is the standard Logan phantom image and  $\mathbf{y}_2$  is a modified image of  $\mathbf{y}_1$  obtained by moving three small anomalies to their symmetric positions with respect to the middle horizontal line. On the other hand, if we add a few low frequencies to 2-skipped subsampling as shown in the image on the right in Fig. 2, the situation is dramatically changed and separability (8) may be achieved. In Fig. 3, we demonstrate the separability again using the real

data. (b) is the ground truth and the tumor is at the bottom. (a) is the reconstructed image using the 2-skipped subsampling; the tumors are found at both top and bottom, and the 2-skipped subsampling is not separable. However, in the reconstructed image (c) using the 2-skipped subsampling with added low frequencies the tumor is clearly located at the bottom and separability (8) may be achieved. This crucial observation is validated by various numerical simulations as shown in Fig. 6.

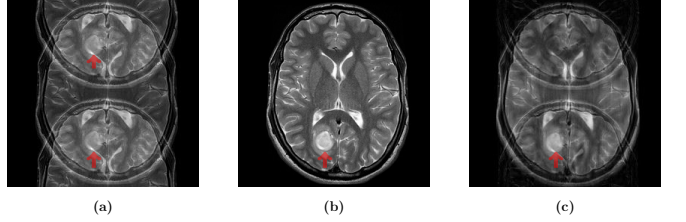


Fig. 3. MR images of human brain with tumor at the bottom. Images are reconstructed from (a) 50% uniform sampling, (b) full sampling, and (c) 50% uniform sampling with some low frequencies added. In (a) the tumors are found at both top and bottom, and there exists a location uncertainty in uniform sampling. However, in the reconstructed image (c) using the 2-skipped subsampling with added low frequencies, the tumor is clearly located at the bottom and the location uncertainty can be removed by adding a few low frequencies in  $k$ -space.

In our subsampling strategy, we use the 4-skip subsampling (25%  $k$ -space data), add a few low frequencies (4%  $k$ -space data), and obtain an acceleration factor of approximately 3.4. Owing to the Poisson summation formula, the 4-skipped data provides the detailed structure of the folded image of  $\mathbf{y}$  as

$$\mathbf{y}_{4\text{-fold}}(n, m) = \sum_{j=0}^3 \mathbf{y}(n, m + \frac{jN}{4}). \quad (9)$$

However, the folded image may not contain location information of small anomalies. We fix the anomaly location uncertainty by adding a minimal amount of low frequency  $k$ -space data. Adding low frequency data provides a highly blurred image along the phase-encoding direction. However, this low-resolution image seems to be sufficient to compensate for the location uncertainty of the high-resolution folded image.

#### B. Image Reconstruction Function

Given a training set  $\{\mathbf{y}^{(j)}\}_{j=1}^M$  of ground-truth MR images, we apply our subsampling strategy  $\mathcal{S}$  to each ground-truth MR image  $\mathbf{y}^{(j)}$  and get the training set  $\{(\mathbf{x}^{(j)}, \mathbf{y}^{(j)})\}_{j=1}^M$  of subsampled data and ground-truth MR images. As shown in Fig. 4, the input  $\mathbf{x}^{(j)}$  of the image reconstruction function  $f$  is an undersampled  $k$ -space data and the output  $\mathbf{y}^{(j)}$  is our reconstruction image. In this subsection, we describe the design of the image reconstruction function  $f$  using deep learning.

We first apply the inverse Fourier transform to the undersampled  $k$ -space data  $\mathbf{x}^{(j)}$ , extract absolute values, and obtain folded images  $\mathbf{y}_s^{(j)}$ . Our goal is then to recover the ground truth images  $\mathbf{y}^{(j)}$  from folded images  $\mathbf{y}_s^{(j)}$ . There is an actively developing deep learning area called the super resolution,

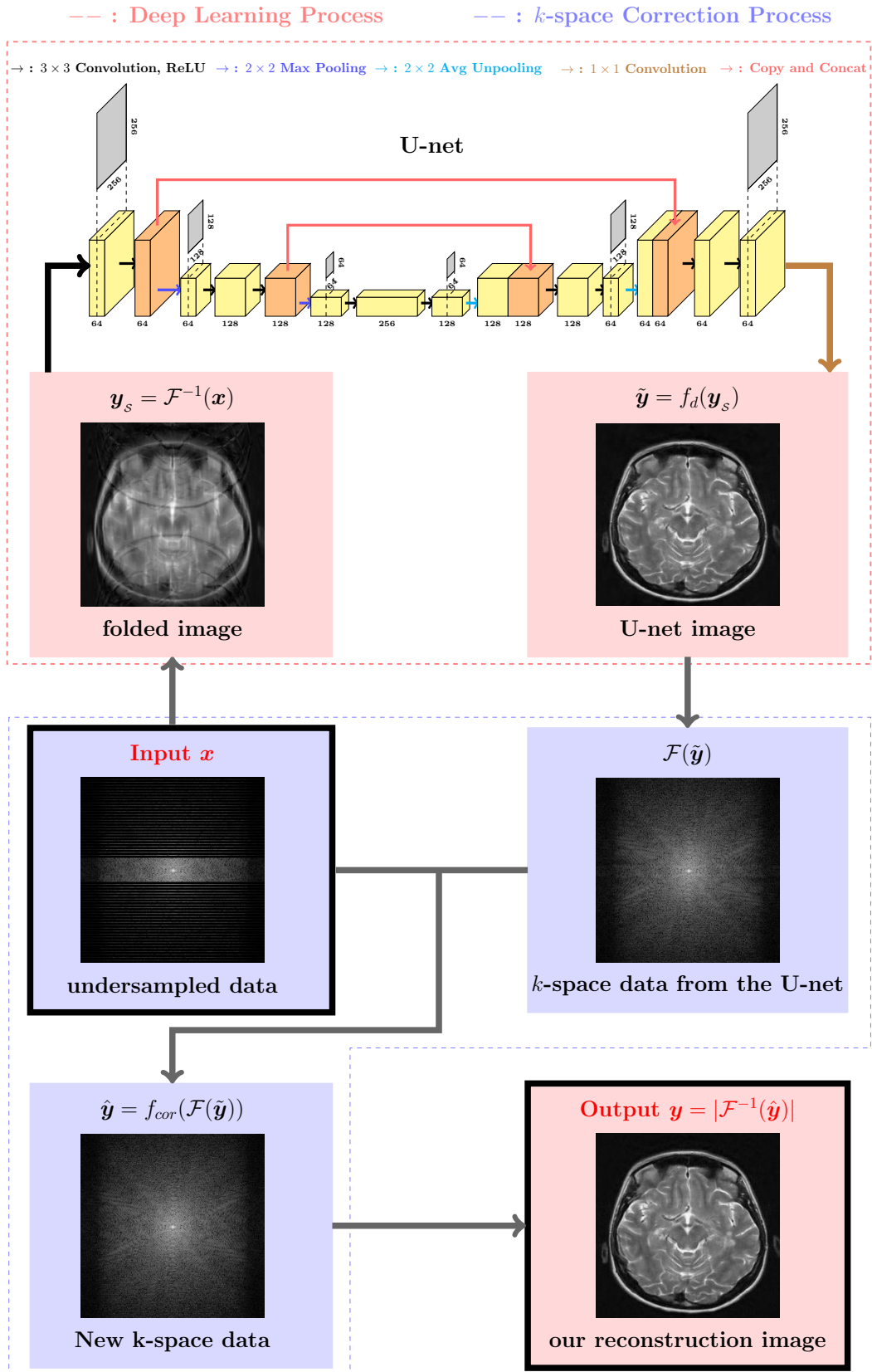


Fig. 4. Overall process of the proposed method including architecture of U-net. The image is first reconstructed by deep learning technique. The U-net image is further tuned by  $k$ -space correction. The final reconstruction is obtained by the inverse Fourier transform of the restored  $k$ -space data.

which enhances the resolution of the poor original images. Our data set is different from the usual data sets handled by the super resolution, but the basic underlying ideas are identical. We search available tools and choose to use U-net, which has quite promising records in the medical imaging field. The architecture of our U-net is illustrated in Fig. 4. The first half of the net is contraction and the last half is expansion. Each step in contraction comprises two convolutions with  $3 \times 3$  windows, a stride 1 in both directions, and zero-padding. After each convolution, we use a rectified linear unit(ReLU) as our activation function, and  $2 \times 2$  max pooling with stride 2. We use zero-padding to equalize the input and label image size. During expansion, we use average unpooling instead of max pooling. After average unpooling, we concatenate a contraction feature map of the same size to the unpooling feature map. The input of the net is  $\mathbf{y}_s^{(j)}$ , the weights is  $W$ , the net as a function is  $f_{net}(\cdot, W)$ , and the output is denoted as  $f_{net}(\mathbf{y}_s^{(j)}, W)$ . To train the net we use the  $L^2$  loss and find the optimal weight set  $W_0$  such that

$$W_0 = \operatorname{argmin}_W \frac{1}{M} \sum_{j=1}^M \|f_{net}(\mathbf{y}_s^{(j)}, W) - \mathbf{y}^{(j)}\|_{L^2}^2. \quad (10)$$

After training, the net as a function is  $f_d = f_{net}(\cdot, W_0)$ , and the output is denoted by  $\tilde{\mathbf{y}}^{(j)} = f_d(\mathbf{y}_s^{(j)}) = f_{net}(\mathbf{y}_s^{(j)}, W_0)$ .

We input the folded image  $\mathbf{y}_s^{(j)}$  into the trained net and obtain the U-net image  $\tilde{\mathbf{y}}^{(j)}$ . We apply the Fourier transform to the U-net image  $\tilde{\mathbf{y}}^{(j)}$  and get the  $k$ -space data  $\mathcal{F}(\tilde{\mathbf{y}}^{(j)})$  from the U-net. Recall that the input  $\mathbf{x}^{(j)}$  is undersampled  $k$ -space data and 71% of  $\mathbf{x}^{(j)}$  are zero-padded. The  $k$ -space data  $\mathcal{F}(\tilde{\mathbf{y}}^{(j)})$  from the U-net recovers the zero-padded part of the information and fills up the numbers. During this recovery,  $\mathcal{F}(\tilde{\mathbf{y}}^{(j)})$  also modifies the non zero-padded parts and distorts the numbers. It is reasonable to keep the original data  $\mathbf{x}^{(j)}$  in the non zero-padded part, change the zeros in the non zero-padded part and fill up the numbers from the  $k$ -space data  $\mathcal{F}(\tilde{\mathbf{y}}^{(j)})$  from the U-net. We call this  $k$ -space correction as  $f_{cor}$  and the new  $k$ -space data  $\hat{\mathbf{y}}^{(j)} = f_{cor}(\mathcal{F}(\tilde{\mathbf{y}}^{(j)}))$ . Since the original input data is preserved, we expect to obtain a more satisfactory reconstruction image. Our experiments show that the  $k$ -space correction is very effective.

Finally, we apply Fourier transform to  $\hat{\mathbf{y}}^{(j)}$  and get our reconstruction image  $\mathcal{F}(\hat{\mathbf{y}}^{(j)})$ . In summary, our image reconstruction function  $f : \mathbf{x} \mapsto \mathbf{y}$  is given by

$$f = |\mathcal{F}^{-1}| \circ f_{cor} \circ \mathcal{F} \circ f_d \circ |\mathcal{F}^{-1}|, \quad (11)$$

where  $f_d$  is the trained U-net and  $f_{cor}$  indicates the  $k$ -space correction.

### III. EXPERIMENT

In our experiment, the ground-truth MR image  $\mathbf{y}$  was normalized to be in the range  $[0, 1]$  and the undersampled data  $\mathbf{x}$  was subsampled to 29%  $k$ -space data as described in Section II. We trained our model using a training set of 1,400 images from 30 patients. Fig. 5 shows the overall structure of our image reconstruction.

To train our deep neural network, all weights were initialized by a zero-centered normal distribution with standard

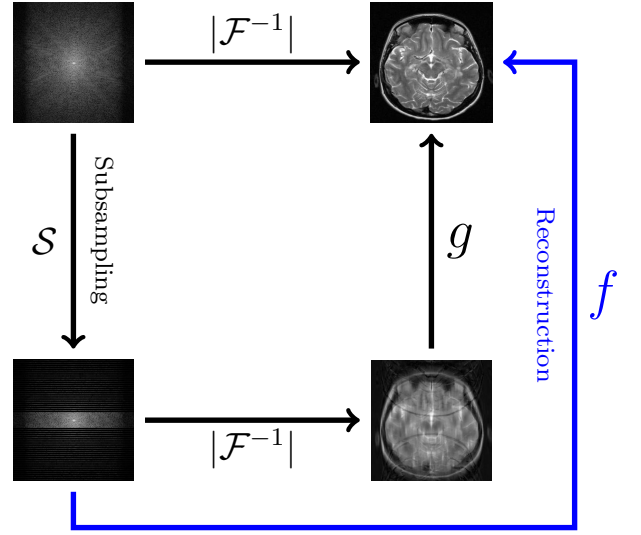


Fig. 5. Schematic diagram of the proposed undersampled reconstruction.

deviation 0.01 without bias term. The loss function was minimized using the RMSPropOptimizer [6] with a learning rate of 0.001, weight decay of 0.9, and mini-batch size of 32 at each epoch. The number of epoch was 2,000. Training was implemented using Tensorflow [4] on an Intel(R) Core(TM) i7-6850K, 3.60GHz CPU and four NVIDIA GTX-1080, 8GB GPU system. The network required approximately 6 hours for training.

Fig. 6 shows the performance of the proposed method for five different brain images in the test set. The first, second and third columns show the ground-truth, aliased and corrected images, respectively. The aliased images are folded four times. Some folds are quite strong and visible, while others are not. The proposed method suppresses these artifacts, but provides surprisingly sharp and natural-looking images.

Fig. 7 displays the impact of  $k$ -space correction. The first, second, third, and last columns represent the ground-truth, aliased, U-net, and  $k$ -space correction images, respectively. The images (c) before and (d) after  $k$ -space correction are visually indistinguishable. In the second row, we display the difference between the images in the column and the ground truth. (e) is the difference between the ground truth and ground truth, and (f) is the difference between the aliased image and ground truth. One can clearly see the folding artifacts. (g) is the difference between the U-net image and ground truth. The U-net eases the folding artifacts dramatically. However, one can still see the folding artifacts. (h) is the difference between the corrected image using  $k$ -space correction and ground truth. The  $k$ -space correction removes the remaining folding artifacts further.

All our observations are supported by the quantitative evaluation. After training, we use the test set of 400 images, and measure and report their mean-squared error (MSE) and Structural Similarity Index (SSIM) [17] in Table I. All these indices strongly support the effectiveness of both the U-net and  $k$ -space correction. In particular, the validity of  $k$ -space

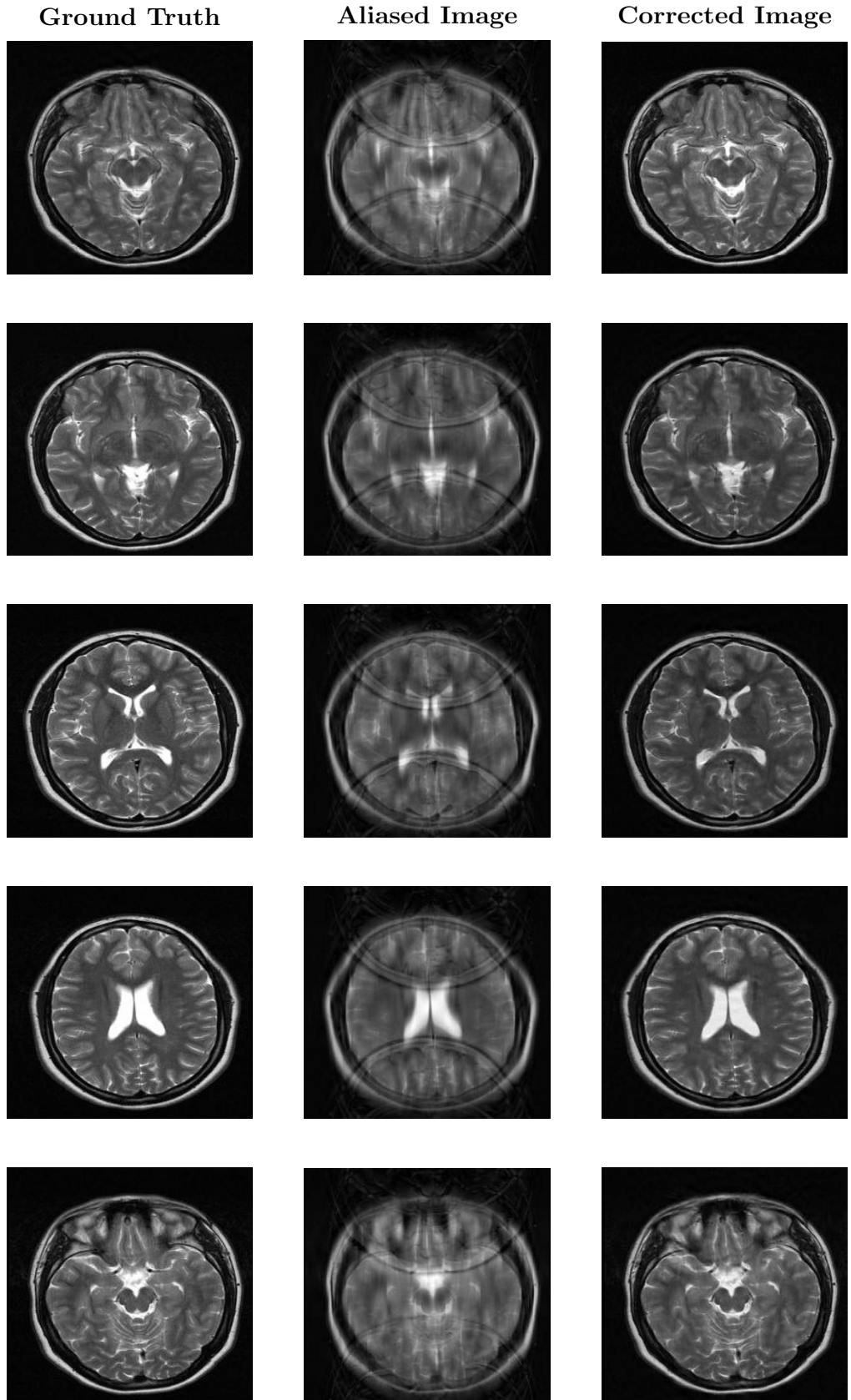


Fig. 6. Numerical simulation results of five different brain MR images. The first, second and third columns show the ground-truth, aliased and corrected images, respectively. The proposed method significantly reduces the undersampling artifacts while preserving morphological information.

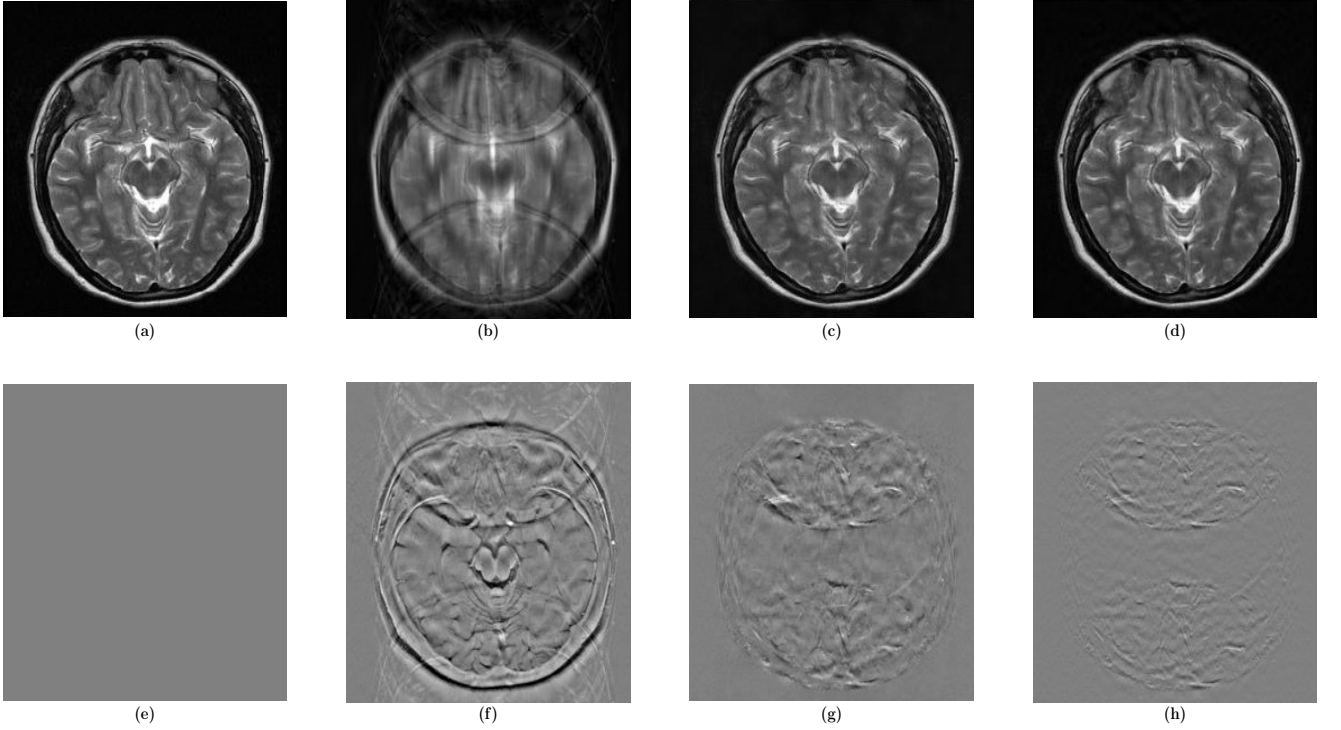


Fig. 7. Simulation result using the proposed method : (a) ground-truth image; (b) aliased image; (c) output from the trained network; (d)  $k$ -space corrected image; Fig. (e)-(h) depict the difference image to the image (a).

correction is justified further.

TABLE I

QUANTITATIVE EVALUATION RESULTS IN TERMS OF MSE AND SSIM  
USING THE TEST SET OF 400 IMAGES.

	Aliased	U-net	Proposed
MSE	$0.0043 \pm 0.0016$	$0.0012 \pm 0.0006$	$0.0004 \pm 0.0002$
SSIM	$0.6516 \pm 0.0815$	$0.8782 \pm 0.0411$	$0.9039 \pm 0.0431$

#### IV. DISCUSSION AND CONCLUSION

Deep learning techniques exhibit surprisingly good performances in various challenging fields and our case is not an exception. In our case, it generates the reconstruction function  $f$  using the U-net, providing a very competitive performance over the existing methods. It should be mentioned that, at the time of writing this paper, we found that there is another work that proposes almost the same approach as [5], [9], [18]. However, in contrast to our paper, no theoretical explanation as to why the undersampled MRI reconstruction works well has been provided.

Our inverse problem of undersampled MRI reconstruction is ill-posed in the sense that there are fewer equations than unknowns. The underdetermined system in Section III has  $256 \times 256$  unknowns and  $76 \times 256$  equations. The dimension of the set  $\{\mathbf{y} \in \mathbb{R}^{256 \times 256} : \mathcal{S} \circ \mathcal{F}(\mathbf{y}) = \mathbf{0}\}$  is  $(256 - 76) \times 256$ , and therefore it is impossible to have an explicit reconstruction formula for solving (6), without imposing a strong constraint of a solution manifold. For the uniqueness, the Hausdorff dimension of the solution manifold must be less than the number

of equations (i.e.,  $76 \times 256$ ). Unfortunately, it is extremely hard to find a mathematical expression for the complex structure of MR images in terms of  $76 \times 256$  parameters, because of its highly nonlinearity characteristic. The deep learning approach is a feasible way to capture MRI image structure as dimensionality reduction.

We learned the kind of subsampling strategy necessary to have a medically acceptable image reconstruction function after extensive effort. Initially we used the 4-skip subsampling, but realized that it could not satisfy the separability condition. We added some low frequencies hoping to satisfy separability and this turned out to guarantee separability in a practical sense.

Once the data set satisfies the separability condition, we have many deep learning tools to recover the images from the folded images. We chose to use the U-net. The trained U-net successfully unfolded and recovered the images from the folded images. The U-net eases the folding artifacts; however, one can still see them. The  $k$ -space correction eases the folding artifacts further.

Numerous experiments show that our learned function  $f$  appears to have highly expressive representation capturing anatomical geometry as well as small anomalies. We also observed that the learned function  $f$  using MRI images solved the undetermined problem (6) for CT images that are never trained. Describing the process of recognizing the features and roles of functions in the learning network with mathematical rigorous analysis will be taken up in future research.

#### ACKNOWLEDGMENT

This research was supported by the National Research Foundation of Korea No. NRF-2017R1A2B20005661.

#### REFERENCES

- [1] E.J. Candès, J. Romberg and T. Tao, "Robust Uncertainty Principles: Exact Signal Reconstruction from Highly Incomplete Frequency Information," *IEEE Trans. Inf. Theory*, vol. 52, no. 2, pp. 489–509, 2006.
- [2] D.L. Donoho, "Compressed sensing," *IEEE Trans. Inf. Theory*, vol. 52, pp. 1289–1306, 2006.
- [3] D.L. Donoho, "For most large underdetermined systems of linear equations the minimal 1-norm solution is also the sparsest solution," *Communications on pure and applied mathematics*, vol. 59, pp. 797–829, 2004.
- [4] Google, "TensorFlow: Large-scale machine learning on heterogeneous systems," URL <http://tensorflow.org/>, 2015.
- [5] K. Hammerl, T. Klatzer, E. Kobler, M.P. Recht, D.K. Sodickson, T. Pock and F. Knoll, "Learning a Variational Network for Reconstruction of Accelerated MRI Data," *arXiv preprint*, arXiv:1704.00447, 2017.
- [6] T. Tieleman and G. Hinton, "Lecture 6.5-rmsprop: Divide the gradient by a running average of its recent magnitude," *COURSERA: Neural Networks for Machine Learning*, 2012.
- [7] D.J. Larkman and R.G. Nunes, "Parallel magnetic resonance imaging," *Phys. Med. Biol.*, vol. 52, pp. R15–R55, 2007.
- [8] P.C. Lauterbur, "Image Formation by Induced Local Interactions: Examples of Employing Nuclear Magnetic Resonance," *Nature*, vol. 242, pp. 190–191, 1973.
- [9] D. Lee, J. Yoo, J.C. Ye, "Deep artifact learning for compressed sensing and parallel MRI," *arXiv preprint*, arXiv:1703.01120, 2017.
- [10] M. Lustig, D.L. Donoho and J.M. Pauly, "Sparse MRI: The Application of Compressed Sensing for Rapid MR Imaging," *Magnetic Resonance in Medicine*, Vol. 58, pp. 1182–1195, 2007.
- [11] H. Nyquist, "Certain topics in telegraph transmission theory," *Trans. AIEE*, vol. 47, pp. 617–644, 1928.
- [12] K.P. Pruessmann, M. Weiger, M.B. Scheidegger and P. Boesiger, "SENSE: sensitivity encoding for fast MRI," *Magn. Reson. Med.*, vol. 42, pp. 952–962, 1999.
- [13] O. Ronneberger, P. Fischer, and T. Brox, "U-net: Convolutional networks for biomedical image segmentation," in *Int. Conf. on Medical Image Computing and Computer-Assisted Intervention*, Springer, pp. 234–241, 2015.
- [14] J. K. Seo and E. J. Woo, "Nonlinear inverse problems in imaging," *Chichester, U.K.: John Wiley & Sons*, 2013.
- [15] J. K. Seo, E. J. Woo, U. Katscher, and Y. Wang, "Electro-Magnetic Tissue Properties MRI," *Imperial College Press*, 2014.
- [16] D.K. Sodickson and W.J. Manning, "Simultaneous acquisition of spatial harmonics (SMASH): fast imaging with radiofrequency coil arrays," *Magn. Reson. Med.*, vol. 38, pp. 591–603, 1997.
- [17] Z. Wang, A. C. Bovik, H.R. Sheikh, E.P. Simoncelli, "Image Quality Assessment: From Error Visibility to Structural Similarity," *IEEE Trans. on Image Processing* Vol. 13, no. 4, pp. 600–612, 2004.
- [18] S. Wang, Z. Su, L. Ying, X. Peng, S. Zhu, F. Liang, D. Feng and D. Liang, "Accelerating magnetic resonance imaging via deep learning," in *Proc. IEEE 13th Int. Conf. Biomedical Imaging*, pp. 514–517, 2016.

APPENDIX. This appendix presents the reconstruction process intuitively using a simplified version of the U-net.

